Soft Matter

Accepted Manuscript

ROYAL SOCIETY OF CHEMISTRY

www.rsc.org/softmatter

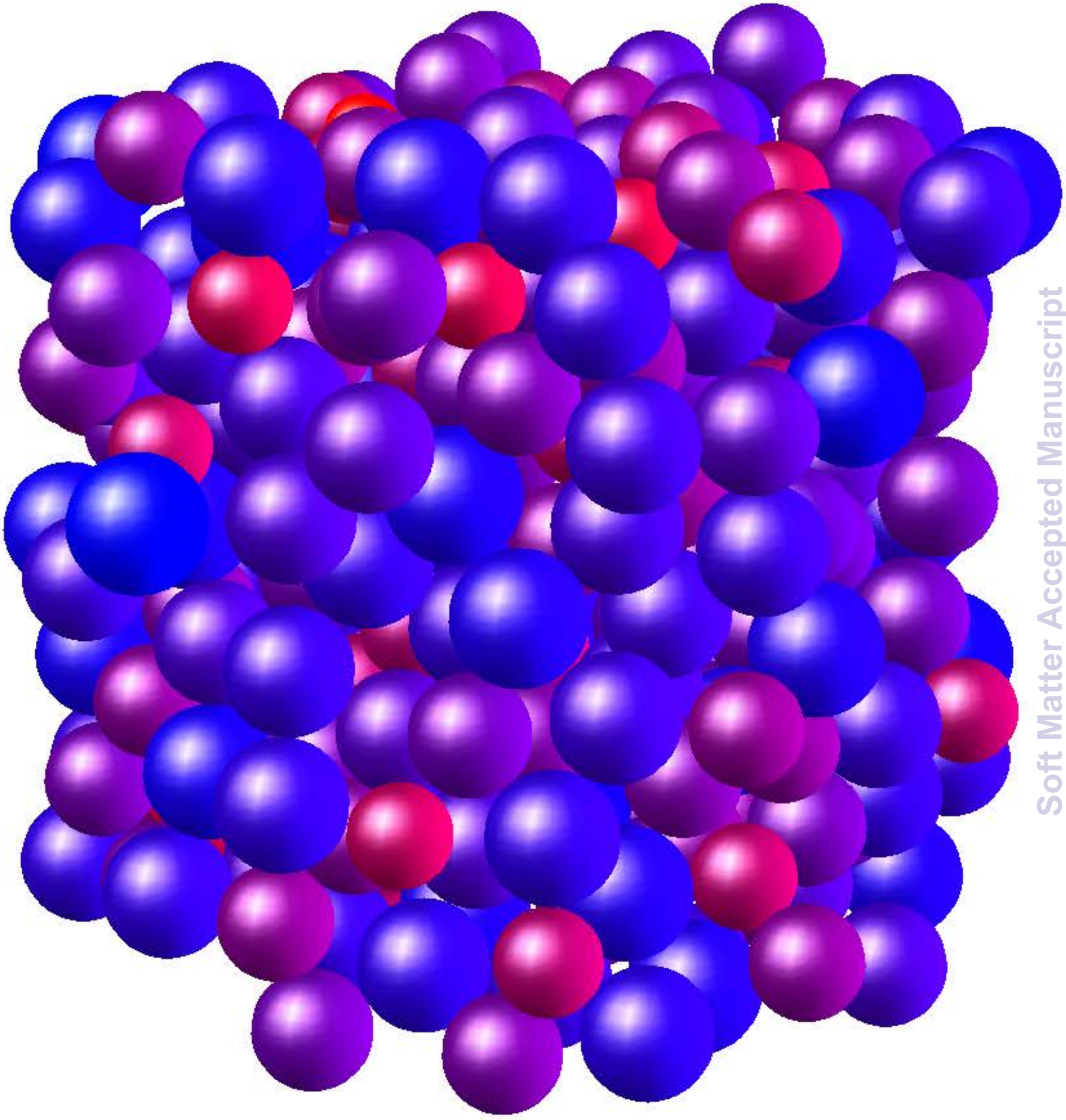

Denser fluids of charge-stabilized colloids form denser sediments

Pilkhaz M. Nanikashvili,[a,b,¶] Alexander V. Butenko,[b,c,¶] Shir R. Liber,[b,c] David Zitoun,[*a,b] and Eli Sloutskin[*b,c]

Granular matter, where solid-like elasticity emerges in absence of crystalline order, has been actively studied in the last decades, targeting fundamental physical understanding of granular packings and glasses, abundant in everyday life and technology. We employ charge-stabilized sub-micron particles in a solvent, known as colloids, to form granular packings through a well-controlled process, where initially homogeneous and thermodynamically equilibrated colloidal fluids form solid sediments, when subjected to an effective gravity in a centrifuge. We demonstrate that particles' volume fraction φ_j in these sediments increases linearly with that in the initial fluid φ_0, setting an upper limit $\varphi_{RCP} \approx 0.64$ on both φ_j and φ_0, where φ_{RCP} coincides with the well-known, yet highly controversial, 'random close packing' density of spheres, providing a new insight into the physics of granular packings. The observed $\varphi_j(\varphi_0)$ dependence is similar to the one recently reported [1] for colloidal hard spheres, sterically-stabilized by surface-linked polymer combs. However, the lower limit on sediment densities drops to $\varphi_j \approx 0.49$ in the present work, suggesting that sedimented charge-stabilized silica are able to overcome mutual electrostatic repulsions, forming gel-like structures stabilized by occasional van der Waals contacts. Finally, by introducing particle size polydispersity, which significantly modifies fluid structure and sedimentation dynamics, we almost completely diminish the $\varphi_j(\varphi_0)$ dependence, bringing $\varphi_j(0)$ close to its value in frictionless systems.

1 Introduction

Solid packings of granular matter, where crystalline periodicity is missing, are abundant in geophysics and technology and play an important role in many fields of science, ranging from astrophysics [2] to information theory and error correction [3]. The tendency of dense granular matter to form these, so-called 'jammed' states can be fruitfully exploited for technological applications [4], such as in slip-casting of ceramics [5] and in selective laser sintering [6]; yet, it also commonly presents a significant nuisance [7], limiting, for example, the transport through a slurry pipeline [8] or discharge from a silo [9]. The physics of jamming transition was intensively studied in the last decades. However, the fundamental mechanism which drives a dramatic emergence of solid-like elasticity at this transition, with the microscopic structure almost unchanged, is still not fully understood, and the relationship between jamming and glass transition in molecular fluids is still being elaborated [10–12]. Moreover, while common glasses are ultimately formed from a finite-density fluid [11,13], which is then driven out-of-equilibrium by rapid cooling [12] or isotropic compression [14], experimental granular packings are typically formed unidirectionally under gravity [15,16], by sequential dropping of individual particles, on random, into a container [17–19]. The possible influence of these preparation procedure differences on density, structure and other static and dynamic properties of non-crystalline solids is almost completely unexplored. Thus it is still unknown whether the experimental information collected for different non-crystalline solids must all be treated on the same foot or possibly separated according to the preparation procedure employed in each case; this ambiguity significantly hampers the progress in development of fundamental physical paradigm of glasses and granular packings [12].

In recent experiments [1], hard colloidal spheres of PMMA [poly(methyl methacrylate)] were used to form solid non-crystalline packings through a unidirectional process, under an effective gravitational acceleration $g_{\mathtt{eff}}$ in a centrifuge. These packings, formed out of finite-density thermodynamically-equilibrated fluids of simple hard spheres, the structures of which were fully characterized by experiment and theory [20], allowed one of the advantages of colloids to be fruitfully exploited: while the state of a colloidal fluid is fully determined by thermodynamics at an ambient gravity $g = 9.8$ m/s^2, the thermodynamics is completely irrelevant in a centrifuge, where Brownian diffusion is negligible compared to sedimentation, so that the Péclet number [1] exceeds 10, like in an out-of-equilibrium system of macroscopic bearings. By starting from fluids of different particle volume fractions φ_0, the same sedimentation process leads to a wide range of different non-crystalline solid packings. The particle volume fraction in sediments formed from the most dilute fluids ($\varphi_0 \to 0$) is $\varphi_j \approx 0.55$, as in the loosest packings of macroscopic marbles, dropped on random, one-by-one, into a container [17–19]; this is known as the 'random loose packing' (RLP) limit [16,21],

[a] *Department of Chemistry, Bar-Ilan University, Ramat-Gan 52900, Israel; E-mail: David.Zitoun@biu.ac.il*
[b] *Institute for Nanotechnology and Advanced Materials, Bar-Ilan University, Ramat-Gan 52900, Israel.*
[c] *Department of Physics, Bar-Ilan University, Ramat-Gan 52900, Israel. E-mail: Eli.Sloutskin@biu.ac.il*
¶ *These authors contributed equally to this work.*

φ_{RLP}. The same process, if started from a denser initial fluid ($\varphi_0 \to 0.64$) leads to much denser sediments, up to so-called 'random close packing' (RCP) limit $\varphi = \varphi_{RCP} = 0.64$. In granular matter experiments, the RCP limit is typically obtained by poorly controlled tapping and shaking, or by inhomogeneous bed fluidization procedures[17,22,23], so that the relation between the RCP and the RLP limits remained unclear and their physical significance was controversial[24]. In particular, it was widely believed that these limits are necessarily related to changes in the number of contacts per particle[25,26]. Colloidal sedimentation experiments[1], where both of these limits can be obtained, depending solely on particle density in the initial fluid, suggest that the RLP corresponds to the maximally random jammed (MRJ) state[24] of highly-frictional spheres, in full agreement with theoretical predictions, obtained either in presence[21] or in-absence[27] of gravity. Importantly, here MRJ denotes the density, for which the number of mechanically-stable states is maximized; other definitions of MRJ, based on minimization of a local order parameter and careful consideration of the jamming category, should lead to similar conclusions[1,24]. Finite density fluids, where the local structure is ordered, form denser (and locally-ordered) sediments, up to φ_{RCP}, suggesting that the structures of solid sediments may be linked with the thermodynamic states of the initial fluids; a simple fully-deterministic computer simulation was constructed along these lines[1], allowing the RLP and the RCP limits to be mutually related. Moreover, this interpretation hints that a common theoretical framework may be constructed to describe both granular packings and glasses. For example, the RLP limit, hitherto observed only in granular packing experiments under gravity, may possibly exist for gravitationless hard frictional spheres[14], if jammed by a rapid compression from zero density; clearly, additional studies are needed to validate these, quite speculative, predictions. Finally, the attribution of the RLP limit to significant friction between PMMA colloids was further supported by direct fluorescent microscopy, demonstrating the Brownian rotation within the sediments to be completely arrested by tangential interparticle forces[1]; recently, the presence of friction was experimentally validated in other colloidal systems[28], which strongly supports our work. With the friction playing an important role in PMMA colloids, sterically-stabilized by poly-12-hydroxystearic acid[29,30], it remained unclear whether a similar $\varphi_j(\varphi_0)$ dependence occurs for charge-stabilized colloids as well, in spite of their tribological properties being markedly different.

In present work, we measure the density of solid packings, prepared by sedimentation in a centrifuge of charge-stabilized SiO_2 colloids from an initially-homogeneous suspension. A linear increase of packing density with the volume fraction φ_0 of the initial fluid is observed, with the maximal density of fluids and sediments limited by $\varphi_{RCP} = 0.64$. Interestingly, sediments of dilute fluids ($\varphi \to 0$) have significantly lower densities than achievable with sterically-stabilized colloids, indicating that van der Waals attractions dominate on close approach between the spheres. As a result, the number Z of force-bearing contacts needed to immobilize a particle is lower than in hard frictional PMMA spheres, where attractive interactions were missing. The observed $\varphi_j(\varphi_0)$ scaling is reproduced by simple computer simulations, which were previously successfully used to describe sediments of hard frictional PMMA spheres[1]. In addition, we demonstrate the effect of particle polydispersity on φ_j; for highly-polydisperse colloids, the slope of $\varphi_j(\varphi_0)$ is significantly reduced. The corresponding increase in $\varphi_j(0)$ is more dramatic than predicted by our simple computer simulations, as also by some other theoretical models, calling for more detailed studies of this effect to be carried out in the future.

2 Experimental details

The synthesis of SiO_2 particles is adapted from the classical work of Stöber[31,32]. Particle size distributions $P(\sigma)$ were obtained from TEM (transmission electron microscopy) images, where ~ 300 particle diameters σ were measured manually, employing the free Fiji software[33]. TEM imaging was carried out with the FEI Tecnai-12 instrument at 120 kV. Samples were prepared by placing a drop of diluted suspension on a 400-mesh carbon-coated nickel grid. A TEM image used for a typical $P(\sigma)$ of monodisperse silica particles is shown in Fig.1, together with the corresponding particle size distribution. Particle polydispersity is commonly defined[34–36] as $\delta \equiv \sqrt{\langle \Delta\sigma^2 \rangle}/\langle \sigma \rangle$, where $\Delta\sigma = \sigma - \langle \sigma \rangle$, and $\langle \sigma \rangle$ is the average particle diameter. A Gaussian fit in Fig. 1(a) matches the experimental distribution for $\delta \approx 0.05$, indicating that the particles are sufficiently monodisperse to exhibit crystallization, if allowed to equilibrate at a high density[36]; therefore, we call this sample in the following 'monodisperse', to distinguish from the higher polydispersity sample (called 'polydisperse' in the following).

For sediment formation studies, SiO_2 particles were dried at 50 ^{o}C; their mass m_p was then determined by weighting, after which the particles were suspended in pure ethanol (Carlo Erba reagents, absolute anhydrous $> 99.9\%$). Particle volume fraction within the suspension of total volume V_s was determined as $\varphi_0 = m_p/(\rho_p V_s)$, where $\rho_p = 1.87 \pm .03$ g/cc was the gravimetric density of the colloids, obtained by applying the Stokes' law to their sedimentation velocity at $\varphi_0 \to 0$. Our value of ρ_p is in a good agreement with the previously published densities of Stöber silica[37–39], which may slightly depend on the details of the preparation protocol[40]. Fluid suspensions of SiO_2 particles were filled into optically-transparent polyamide cuvettes, having a rectangular cross-section of 2×8 mm, such that the filling height was $L_0 \approx$

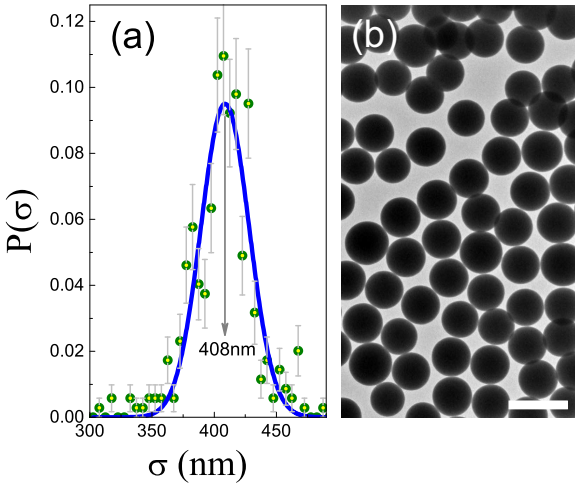

Fig. 1 (a) A typical particle size distribution for the monodisperse SiO_2 spheres, where the solid curve is a Gaussian function. The corresponding TEM image is shown in section (b), where the scale bar length is 600 nm.

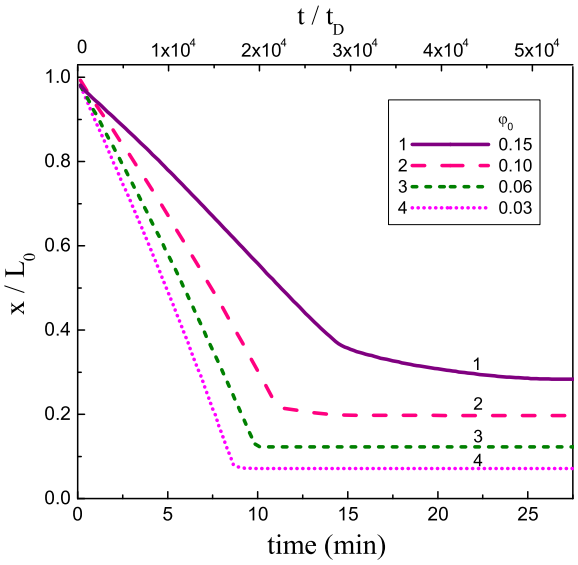

Fig. 2 Sedimentation front positions for monodisperse SiO_2 colloids, $\langle\sigma\rangle = 408$ nm, obtained at an effective gravity of $g_{\mathtt{eff}} = 520g$. Note the sharp slope transitions in the bottom curves at $t = t_c \approx 10$ min, followed by the time-independent regime. These features indicate that the sedimentation process is completed at $t = t_c$, so that no further changes occuring in the system. The post-transitional rounding at $\varphi_0 = 0.15$ is attributed to a possible formation of an intermediate phase, which was not observed for the hard spheres [1].

25 mm; for the macroscopic cuvettes, the results of this work are independent on either the cross-section of the cuvette or the filling height [1]. The suspensions were vigorously shaken on a commercial vortexer, then placed horizontally into the LUMiFuge analytical centrifuge, which measures light transmission profiles $I(x',t)$ through the samples at a wavelength of 870 nm, in situ, during centrifugation [1]; here x' is the distance from the bottom of the sample and t is the time passed after the beginning of centrifugation. When the sediment is fully formed, the ratio between its volume and the volume of the initial fluid sample is equal, by volume conservation, to φ_0/φ_j, where φ_j is the particle volume fraction within the sediment; thus, with the φ_0 known from sample preparation procedures, φ_j is readily obtained by simple measurements of sample volume.

3 Results and Discussion

3.1 Sediments of monodisperse particles

To directly examine the dynamics of the sedimentation process, we measure the position of the sedimentation front $x(t)$, separating the sedimenting fluid suspension and the particle-free solvent, known as supernatant. At early centrifugation times, the front position is linear in time, indicating that colloidal sedimentation velocity is constant, see Fig. 2. A similar behavior was observed for the PMMA particles, where the sedimentation velocities, for a wide range of centrifugal accelerations, were described by the classical Stokes' law, modified to account for the viscosity of dense colloidal suspensions being higher than that of the pure solvent; this effective medium theory, which describes our current results as well, was used to extract the particle volume fraction φ_0 in colloidal suspensions of PMMA. SiO_2 spheres, used in the current work, are advantageous in that they do not swell in organic solvents, so that φ_0 is obtained by simple weighing of the dried particles, increasing the reliability of the absolute values of φ_0; recent controversy with respect to the validity of the effective medium theory in some colloidal systems [42] further emphasizes the importance of this independent procedure for the determination of φ_0. Since φ_0 values are used to extract the particle volume fractions within the sediments φ_j, the overall reliability of $\varphi_j(\varphi_0)$ scalings is significantly increased for silica particles, providing support to our previous work [1].

The linear decrease in $x(t)$ halts by a sharp transition at $t = t_c$, with the front positions being time independent for $t > t_c$, as shown in the bottom curves in Fig. 2. The sharpness of this transition indicates that the sedimentation process is fully completed by $t = t_c$ and no additional compression of the sediment takes place, except possibly for the denser suspensions (upper curve in Fig. 2), where slight post-transitional rounding of $x(t)$ is detected. No similar rounding was observed for hard PMMA spheres [1], suggesting that much softer Coulombic interactions between charge-stabilized silica spheres may be responsible for this phenomenon. In particular, assuming

that the sediment is homogeneous at $t = t_c$, as for the lower φ_0, we obtain the separation between particle surfaces at t_c to be ~ 30 nm, close to the Debye lengths previously-reported for similar suspensions[43,44]. Thus, the rounding at $t > t_c$ may indicate formation of a colloidal 'Wigner' glass phase[45], stabilized by Coulombic repulsions. Future studies, employing suspensions in a wide range of Debye lengths and centrifugation rates, should allow the nature of the observed post-transitional rounding to be elucidated. At present, we disregard this rounding and take the $x(t \to \infty)$ limit for the height of our solid sediments. Importantly, if an intermediate phase does indeed form, the structure of this phase does not undergo significant relaxation on experimentally-relevant timescales, as evidenced by the $\varphi_j(\varphi_0)$ scaling (see below) being similar both in presence ($\varphi_0 > 0.15$) and in absence ($\varphi_0 < 0.15$) of post-transitional rounding.

A common assumption in colloidal physics[46] is that the density of all colloidal sediments is equal to $\varphi_{RCP} \approx 0.64$, regardless of the density of the initial fluid. To test this assumption, we directly measure the average particle volume fractions in sediments of charge-stabilized monodisperse SiO_2 spheres. Our experiments demonstrate that sediments of low density fluids are much less dense than commonly assumed, so that $\varphi_j(\varphi_0 \to 0) = 0.490 \pm 0.006$, as demonstrated in Fig. 3 (green circles). Moreover, $d\varphi_j/d\varphi_0 > 0$, with denser fluids forming denser sediments, indicating that short-range order (i. e. coordination shell structure) emerging in finite density fluids induces similar ordering within the sediments. A similar behavior was recently observed for sterically-stabilized PMMA spheres[1], albeit with a lower slope $d\varphi_j/d\varphi_0$ (purple dashes in Fig. 3); the consequent bottom limit on sediment density was obtained there as $\varphi_j(0) \approx 0.55 \pm 0.02$, indicating that particle interactions play an important role in determination of φ_j. Indeed, a much lower value of $\varphi_j(0) \approx 0.15$ is obtained in solid agglomerates formed by random ballistic deposition (RBD) of SiO_2 microspheres under vacuum[2]; in an RBD process, where particle impact velocities are of the order of 1-2 m/s, higher by orders of magnitude compared to our work, silica particles exhibit a 'hit-and-stick' behavior, so that one contact with the agglomerate is sufficient for their immobilization (green square in Fig. 3). Finally, frictionless monodisperse emulsion droplets[47] pack to $\varphi_j = \varphi_{RCP} = 0.64$, and do not exhibit any experimentally-significant variation with the density of the initial fluid, $d\varphi_j/d\varphi_0 \approx 0$. This suggests that the different number of contacts Z required to immobilize frictional ($Z = 4$), friction*less* ($Z = 6$), and sticky ($Z = 2$) spheres determines the $\varphi_j(0)$ value; the emergence of solid-like properties in granular matter is then related to isostatic conditions, where the number of constraints in the system exactly matches the total number of degrees of freedom.

3.2 Computer simulations

To gain a deeper understanding of the role played by the isostaticity in our sediments, we reproduce the experimental $\varphi_j(\varphi_0)$ by a simple computer simulation[1]. In this simulation, the sedimentation process is taken to be fully deterministic and hydrodynamic interactions are totally neglected, for simplicity. First we simulate fluids of simple hard spheres at different volume fractions; the structure of these fluids perfectly matches the predictions of the classical Percus-Yevick approximation[20], confirming that the system is fully equilibrated. Initially, the boundary conditions are chosen to be periodic, in all three dimensions. The number of particles N was chosen to be between 4×10^3 and 10^5. The xy-dimensions of the cell ($L \times L$) were either 10×10 or 30×30 (in σ units), while the size of the simulation cell in z-direction was larger, determined by φ_0 and N; the results do not significantly depend on either N or L in our range of values. To prepare a sediment out of this simulated fluid, we let the particles 'fall', one by one, along the $-z$ direction. Particles at a lower z are the first to fall. A particle stops falling when it either has a sufficient number of supports ζ from particles which already belong to the sediment or when it reaches $z = 0$. Importantly, the average number of supports per particle is directly related to the average number of contacts Z per particle: $\langle\zeta\rangle = \langle Z\rangle/2$, by symmetry. A contact between particles is established[26,48] when the separation between their centers is below 1.005 (in σ units). We have carried out simulations with the number of supports per particle ζ being chosen as either 1, 2, or 3; thus, the total number of contacts per particle Z was 2, 4, or 6 (see Fig. 3). For $\zeta > 1$, when a falling-down particle forms its first contact with a particle from the sediment, it moves along the surface of this particle. Then it either falls further down or establishes a contact with an additional particle. For $\zeta = 2$, once this additional contact is established, the particle stops; this particle is then considered to belong to the sediment. For $\zeta = 3$, when the second contact is established, the particle continues to move along the surface of both of its supporting particles. Then it either falls further down, or establishes its third contact with the sediment. Our algorithm is equivalent to the well-known 'dropping and rolling' method of simulations[6,49,50], but does not test the final configuration of each particle for mechanical stability. Note, this sedimentation algorithm is fully deterministic, except for starting from a random instantaneous state of the initial fluid; moreover, with the initial fluid being thermodynamically-equilibrated, the structure of its instantaneous states is well-understood, tested experimentally[20], and described by classical analytical theories[20]. The particle volume fraction profiles $\varphi_j(z)$ along the sediments are typically perfectly flat, except for a couple of particle monolayers at the bottom ($z = 0$). Similar z-independent φ_j is observed by confocal microscopy of PMMA sediments, where the $z = 0$ region

of the sample cell cannot be approached sufficiently closely for the possible formation of monolayers there to be tested. Therefore, in our simulation, we exclude the few monolayers forming at the bottom of the cell; then, the hard volume of the particles within the flat-$\varphi_j(z)$ region of the sediment is divided by the volume of this region, yielding the average volume fraction φ_j. Other ways of extracting φ_j from the simulated profiles were attempted as well; the same results were obtained in each case [1].

To test the validity of our simple simulations, we plot the simulated $\varphi_j(\varphi_0)$ on top of the experimental data in Fig. 3, see solid orange and magenta lines for $Z = 2$ and $Z = 4$ respectively. Remarkably, the simulated φ_j are linear in φ_0, with the slope for $Z = 4$ almost coinciding with that of the experimental hard frictional PMMA spheres [1]; this result is in agreement with the isostatic conditions for frictional spheres being matched for $Z = 4$. The sediments at $Z = 2$ are less dense, forming string-like structures, as demonstrated in Fig. 4 and in the Supporting video file. In particular, our simulations for $Z = 2$ converge to the random ballistic deposition limit at $\varphi_0 = 0$, reproducing experimental (Fig. 3, green square) and theoretical (not shown) φ_j obtained in the 'hit-and-stick' regime [2]. For $Z = 6$, the packing density is high and almost independent of the fluid density [1], as in packings of frictionless emulsion droplets [47] (not shown).

3.3 Discussion

Our simulations connect, through a fully-deterministic algorithm, the instantaneous configurations of the initial thermodynamically-equilibrated simple fluid of hard spheres with the structures of the sediments; each configuration of the fluid, characterized by positions of all particles, leads to one certain, fully-determined, state of the sediment. Conversely, different fluid states may, in some cases, form exactly the same sediment structure. Thus, each fluid configuration belongs to a certain basin of attraction; such basins of attraction are characterized by the sediment structure which eventually forms for the fluid states belonging to the basin. Importantly, there may be more than one sediment structure of a given density; we denote the number of (mechanically-stable) sediment structures of density φ_j by $\Omega_s(\varphi_j)$. In particular, for frictional particles, where the isostaticity is attained at $Z = 4$, this function peaks at $\Omega_s(\varphi_j) \approx 0.55$, the MRJ density of the frictional spheres [21,27] (see blue line in Fig. 5). Also, the basins of attraction differ by their size: the denser is the sediment state, the more free volume does it leave in a fluid of a given density φ_0; therefore, basins of attraction corresponding to denser sediments have, at a given φ_0, a larger volume in the multidimensional phase-space of the fluid. The particles in a fluid at a thermodynamical equilibrium move around, so that, by ergodicity, all energetically-accessible microstates (i.e., the ones where hard spheres do not overlap), belonging to all different basins of attraction, are being visited with the same probability. Thus, the most probable sediment density is the one for which the total volume of the attraction basins is maximal for a given φ_0; similarly, the average sediment density is obtained by averaging through all possible sediment states, weighted by the volume of the corresponding basins of attraction.

For sediments formed by dropping of individual uncorrelated particles ($\varphi_0 = 0$), all the volume is free in the fluid phase, so that the sediment density is determined solely by $\Omega_s(\varphi_j)$. Therefore, for frictionless particles, where the isostatic conditions correspond to $Z = 6$, the most dilute fluids form sediments [24] at $\varphi_j \approx 0.64$ (red line in Fig. 5), as observed in packings of liquid emulsion droplets [47]. Highly frictional particles pack less densely, so that $\varphi_j(0) = \varphi_{RLP} \approx 0.55$ (see purple dashes in Fig. 3) corresponds to the maximum [21,27] of the solid blue line in Fig. 5. Sticky particles, such as in the RBD experiments [2] form loose packings [as in Fig. 4(b)], where $\varphi_j(0) \approx 0.15$, corresponding to the maximum of the black line in Fig. 5. Charge-stabilized SiO_2 particles in a solvent (green symbols in Fig. 3) must overcome significant mutual electrostatic repulsions (Coulomb barrier) to approach each other sufficiently closely to stick by the van der Waals forces [51,52]; thus, 'hit-and-stick' conditions are not met, and $\varphi_j(0)$ is increased significantly compared to the RBD, but still remains lower than φ_{RLP}. Finally, while the exact shapes of Ω_s distributions in Fig. 5 are yet unknown, Ω_s must be the broadest for the sticky particles and the narrowest for the frictionless ones; indeed the set of frictionless packings is fully included into the wider sets of frictional or sticky packings, substantiating the schematic description in Fig. 5.

While $\varphi_j(0)$ values depend solely on Ω_s, in finite density fluids the free volume ΔV_f is increased for structures corresponding to the attraction basins of denser sediments (green dashes in Fig. 5) and, by geometry, attraction basins vanish for $\varphi_j < \varphi_0$. Therefore, the attraction basins of denser sediments are visited more frequently, and the sediment densities are shifted to higher values, as in Fig. 3. This positive biasing of denser sediments leads to the most dramatic consequences for the sticky particles, where Ω_s is the widest; note the significant increase in simulated $\varphi_j(\varphi_0)$ for $Z = 2$ (orange line in Fig. 3). The increase for frictionless particles must be much smaller, in agreement with experiment [47] and simulation (Fig. 4 in Liber *et al.* [1]). While the physical reason for the linear $\varphi_j(\varphi_0)$ dependence, clearly observed in both experimental and simulated data in Fig. 3, is still not clear, this dependence may possibly provide an important insight onto the actual shape of Ω_s. In addition, the extraction of Ω_s from $\varphi_j(\varphi_0)$ may also provide the clue for the absolute φ_j values in our present simulations, as also in previous dropping and rolling simulations [6,49], being too low, as mentioned in the caption to Fig. 3. Interestingly, a very different shape of $\varphi_j(\varphi_0)$ was ob-

tained in computer simulations of isotropically-compressed, gravitationless, frictional Hertz-Mindlin particles[41]; the corresponding data are shown in royal blue rhombi in Fig. 3. Also, the distribution of φ_j about the average, for each value of φ_0, may contain valuable information. Interestingly, this distribution is much narrower for the monodisperse SiO_2 spheres, studied in the present work, compared with the distribution observed earlier for PMMA[1]. We suggest that the size of our currently-used SiO_2 colloids, being $\sim$ 6-fold smaller than that of the previously-used PMMA, allows better averaging of micro-structures within the samples, the size of which was roughly the same in both studies; future experiments will address this issue in a more systematic manner.

Linear $\varphi_j(\varphi_0)$ scalings imply that an upper limit exists for sediment and fluid densities, imposed by the intersection with the $\varphi_j = \varphi_0$ line (shown in grey in Fig. 3); by geometry, sediments must be denser compared with the initial fluids, so that $\varphi_j > \varphi_0$. Strikingly, this intersection yields the same limit for all data in Fig. 3, $\varphi_0 \leq \varphi_j \leq \varphi_{RCP} \approx 0.64$, regardless of the interparticle interactions, suggesting that the limit is set by the properties of the colloidal fluid phase, rather than these of the various sediments. Indeed, within the fluid phase, our colloids are stable, so that frictional and sticky interactions[53] are irrelevant. Therefore, a strong drop[54] in the number of non-frictional fluid states at $\varphi_0 > \varphi_{RCP}$, stemming from the peak in non-frictional $\Omega_s(\varphi_j)$ at $\varphi_j = \varphi_{RCP}$, sets the upper limit on the density of our fluids, where crystallization tendencies are fully suppressed by rapid centrifugation.

Finally, we note that our present simulations assume the particles in the fluid to behave as true hard spheres and neglect hydrodynamic interactions during the sedimentation. These apparently oversimplified assumptions are justified in view of earlier sedimentation studies, demonstrating that hydrodynamic interactions in sedimenting fluids, inducing velocity fluctuations, simply raise the effective temperature of these fluids[55]. At a sufficiently high (effective) temperature, soft electrostatic repulsions between SiO_2 do not matter for the fluid structure, which is then fully determined by the hard steric potentials. Importantly, the microscopic structure of the fluids of hard spheres, where energy scale is missing, is temperature-independent[20,36], suggesting that the details of hydrodynamic velocity fluctuations do not matter for sediment structure determination, as indeed observed from the independence[1] of φ_j on $g_{\mathtt{eff}}$, within the experimentally-accessible range.

In conclusion, our tentative interpretation identifies $\varphi_j(0)$ with the MRJ state, where $\Omega_s(\varphi_j)$ is peaking; therefore, $\varphi_j(0)$ is sensitive to cohesion and friction which change the isostatic conditions. The positive slope of $\varphi_j(\varphi_0)$ is attributed to biasing towards denser sediments in finite density fluids, where free volume considerations apply; thus, for the monodisperse SiO_2, the slope is intermediate between 'hit and stick' ($Z = 2$) and frictional ($Z = 4$) conditions. Finally, the φ_{RCP} limit is associated with the rapid drop in the number of accessible frictionless states, with Ω_s at high φ_j being very similar for all particle interactions.

3.4 Sediments of polydisperse particles

In addition to the 'monodisperse' samples, discussed above, where $P(\sigma)$ was single-peaked and relatively sharp, we also carried out similar sedimentation experiments employing samples with much wider, four-peaked, asymmetric particle size distribution (Fig. 6). For this polydisperse sample we obtain $\delta \approx 0.09$; importantly, this distribution also exhibits a significant skewness[35] $S \equiv \left\langle \Delta\sigma^3 \right\rangle / \left\langle \Delta\sigma^2 \right\rangle^{3/2} = -1.8$, as observed from the highly asymmetric envelope of $P(\sigma)$, where small particles $\sigma < \langle\sigma\rangle$ are under-represented. Breadth and asymmetry of $P(\sigma)$ are known[6,25,34,35,49,50,56–58] to have an influence onto the packing density of spheres, necessitating the TEM analysis carried out in this work.

The $\varphi_j(\varphi_0)$ of the polydisperse particles are shown in cyan circles in Fig. 3, where sediment densities are significantly higher than in the monodisperse case, such as if the smaller particles effectively 'lubricate' the contacts between the larger ones[34], shifting the value of Z at the isostaticity conditions. While the upper limit on sediment densities φ_{RCP} is the same, within experimental accuracy, for both polydisperse and monodisperse particles, polydispersity significantly lowers $d\varphi_j/d\varphi_0$ and increases $\varphi_j(0)$; also, interestingly, the scatter of $\varphi_j(\varphi_0)$ values increases dramatically.

To test the physical origin of the dramatic increase in $\varphi_j(0)$, we modify our simulation algorithm to allow for the polydispersity of the particles. Importantly, since simulation of fluid structures in presence of polydispersity is highly non-trivial[34], we limit the simulations to $\varphi_0 \to 0$, so that the only effect of polydispersity is in formation of mechanical contacts between the particles, on approach to the solid sediment. The resulting $\varphi_j(0)$, for Gaussian $P(\sigma)$ in a wide range of polydispersities, significantly underestimates the experimental value for either $Z = 4$ or $Z = 2$; see open black squares (simulation) and solid blue circle (experiment) in Fig. 7, where the data are normalized by the density of corresponding sediment at zero polydispersity, $\delta = 0$. The range of Gaussian $P(\sigma)$ was limited in each case[6,34] to $\sigma > 0$, albeit for the currently used δ and system sizes this may not be necessary[25].

Recent studies[35] suggest that the shape of $P(\sigma)$, not just its width, may be important for the density of solid amorphous packings; therefore, we have repeated the simulations with the experimental four-peaked $P(\sigma)$ employed, instead of the simple Gaussian one. This did not significantly change the result in our case. Finally, we also attempted to account for particle size separation during the centrifugation, which makes the concentration of larger particles be higher at the bottom of the

sediment, while being lower at its top. For that purpose, we have calculated, for each particle in the fluid, the time τ of its approach to the surface of the sediment; τ is equal to the ratio of the initial height of the particle above the sediment and its Stokes' sedimentation velocity. Then, the usual drop-and-roll algorithm was employed, with the list of particles ordered according to their τ values. A simpler version of algorithm, where larger particles were always the first to reach the sediment was attempted as well. Unfortunately, any of these modifications makes only a very small difference for the value of $\varphi_j(0)$, as demonstrated by the open red square in Fig. 7, calculated employing the experimental $P(\sigma)$ of Fig. 6(a). This procedure does not significantly modify $\varphi_j(0)$ at $Z = 2$ either, as shown in the inset. Finally, while our simulated shifts in $\varphi_j(0)$ with δ are in close agreement with the corresponding shifts in φ_{RCP}, simulated by others (see Fig. 7), they significantly underestimate the experimental result. By contrast, the experimental φ_{RCP} does not vary with δ, within the accuracy of (quite scattered) $\varphi_j(\varphi_0)$ of our polydisperse silica; this result is in agreement with the simulations, where the $\varphi_{RCP}(\delta)$ variation is very weak.

The reason for the experiment-theory mismatch in the case of polydisperse particles is not clear, and may have to do with the subtleties of the sedimentation process, neglected in simulation. In particular, when particle sizes and, consequently, their sedimentation velocities, significantly differ, particle collisions during the centrifugation may lead to formation of dumbbells, which are expected to pack (in a non-crystalline sediment) much denser than the spheres do[59]. Also, our simulations neglect the mutual geometric orientation of contacts immobilizing a particle, so that only the total number of contacts matters and the actual mechanical stability of the particle is not tested; while this approximation works reasonably well for the monodisperse particles, it may be failing dramatically when small particles occasionally support the larger ones, so that the probability for mechanically-unstable configurations is much higher. Clearly, additional theoretical effort is needed to fully understand systems with wide and asymmetric $P(\sigma)$.

4 Conclusions

We have demonstrated that the densities of solid non-crystalline sediments of charge-stabilized SiO_2 colloids, prepared by rapid centrifugation, so that the crystallization is avoided, vary with the density of the initial fluids. The dense fluids form denser sediments, up to the limit of $\varphi_{RCP} \approx 0.64$. The scaling of sediment densities is reminiscent of the one which was obtained earlier for sterically-stabilized hard frictional spheres; however, some quantitative differences, related to the differences in corresponding particle interaction potentials, were observed. In addition, our experiments have tested the impact of a highly-polydisperse and skewed particle size distribution on sediment densities, indicating a significant densification of loose sediments, with no similar change for the denser ones. We have demonstrated that a simple computer simulation, where the sedimentation process is fully deterministic, links sediment densities with the structures of the initial fluid suspensions, which are in a thermodynamic equilibrium and quite well understood. We suggest a common tentative framework, explaining on a qualitative level the relation between RLP and RCP packings, as also the relation between packings of frictional, frictionless, and sticky spheres. In particular, the packings of very dilute fluids $\varphi_0 \to 0$ are suggested to correspond to the MRJ densities, which depend on frictional[28] and cohesion forces between the particles; these loose packings stay in contrast with the ones at the RCP limit, where particle potentials and contact numbers do not matter. Clearly, further validation, by theory and experiment, is needed to substantiate this framework. In particular, the linear $\varphi_j(\varphi_0)$ scalings observed in the present work should allow a deeper insight into the statistical mechanics of microstructures in colloidal sediments, the structure of which can also be directly tested by direct optical microscopy; research in these directions is currently in progress.

5 Acknowledgements

We thank Y. Roichman, Y. Shokef, and M. Wyart for fruitful discussions. E. S., A. V. B., and S. R. L. thank the Israel Science Foundation (#85/10, #1668/10) for funding. P. M. N. thanks the Ministry of Absorption for funding.

References

1 S. R. Liber, S. Borohovich, A. V. Butenko, A. B. Schofield, and E. Sloutskin, *Proc. Natl. Acad. Sci. USA*, 2013, **110**, 5769-5773.

2 J. Blum and R. Schräpler, *Phys. Rev. Lett.*, 2004, **93**, 115503.

3 J. H. Conway and N. J. A. Sloane, *Discrete Comput. Geom.*, 1995, **13**, 383-403.

4 E. Brown, N. Rodenberg, J. Amend, A. Mozeika, E. Steltz, M. R. Zakin, H. Lipson, and H. M. Jaeger, *Proc. Natl. Acad. Sci. USA*, 2010, **107**, 18809-18814.

5 F. Singer and S. S. Singer, *Industrial Ceramics* (Chapman and Hall, USA, 1971).

6 Y. Shi and Y. Zhang, *Appl. Phys. A*, 2008, **92**, 621-626.

7 H. J. Herrmann, J.-R Hovi, and S. Luding, (Eds.), Physics of Dry Granular Media (Kluwer, Dordrecht, 1998).

8 M. Roco and C. A. Shook, *Can. J. Chem. Engng.*, 1983, **61**, 494-503.

9 I. Zuriguel, A. Garcimartín, D. Maza, L. A. Pugnaloni, and J. M. Pastor, *Phys. Rev. E*, 2005, **71**, 051303.

10 A. J. Liu and S. R. Nagel, *Nature*, 1998, **396**, 21-22.
11 G. Parisi and F. Zamponi, *Rev. Mod. Phys.*, 2010, **82**, 789-845.
12 L. Berthier and G. Biroli, *Rev. Mod. Phys.*, 2011, **83**, 587-645.
13 M. Leocmach and H. Tanaka, *Nat. Commun.*, 2012, **3**, 974.
14 Z. Zhang, N. Xu, D. T. N. Chen, P. Yunker, A. M. Alsayed, K. B. Aptowicz, P. Habdas, A. J. Liu, S. R. Nagel, and A. G. Yodh, *Nature*, 2009, **459**, 230-233.
15 M. Clusel, E. I. Corwin, A. O. N. Siemens, and J. Brujić, *Nature*, 2009, **460**, 611-615.
16 K. A. Newhall, I. Jorjadze, E. Vanden-Eijnden, and J. Brujic, *Soft Matter*, 2011, **7**, 11518-11525.
17 J. D. Bernal, *Proc. R. Soc. London, Ser. A*, 1964, **280**, 299-322.
18 G. Y. Onoda and E. G. Liniger, *Phys. Rev. Lett.*, 1990, **64**, 2727-2730.
19 G. R. Farrell, K. M. Martini, N. Menon, *Soft Matter*, 2010, **6**, 2925-2930.
20 P. J. Lu, M. Shutman, E. Sloutskin, and A. V. Butenko, *Opt. Express*, 2013, **21**, 30755-30763.
21 M. Pica Ciamarra and A. Coniglio, *Phys. Rev. Lett.*, 2008, **101**, 128001.
22 M. Jerkins, M. Schröter, H. L. Swinney, T. J. Senden, M. Saadatfar, T. Aste, *Phys. Rev. Lett.*, 2008, **101**, 018301.
23 M. Schröter, D. I. Goldman, and H. L. Swinney, *Phys. Rev. E*, 2005, **71**, 030301(R).
24 S. Torquato and F. H. Stillinger, *Rev. Mod. Phys.*, 2010, **82**, 2633-2672.
25 M. J. Powell, *Powder Technol.*, 1980, **25**, 45-52.
26 K. J. Dong, R. Y. Yang, R. P. Zou, X. Z. An, and A. B. Yu, *Europhys. Lett.*, 2009, **86**, 46003.
27 L. E. Silbert, *Soft Matter*, 2010, **6**, 2918-2924.
28 T. Still, C. P. Goodrich, K. Chen, P. J. Yunker, S. Schoenholz, A. J. Liu, and A. G. Yodh, *Phys. Rev. E*, 2014, **89**, 012301.
29 E. Janai, A. B. Schofield, and E. Sloutskin, *Soft Matter*, 2012, **8**, 2924.
30 L. Antl, J. W. Goodwin, R. D. Hill, R. H. Ottewill, S. M. Owens, S. Papworth, and J. A. Waters, *Colloid Surface*, 1986, **17**, 67.
31 W. Stöber, A. Fink, and E. Bohn, *J. Colloid Interf. Sci.*, 1968, **26**, 62.
32 N. M. Abrams and R. E. Schaak, *J. Chem. Ed.*, 2005, **82**, 450-452.
33 J. Schindelin *et al.*, *Nat. Methods*, 2012, **9**, 676-682.
34 W. Schaertl and H. Sillescu, *J. Stat. Phys.*, 1994, **77**, 1007-1025.
35 K. W. Desmond and E. R. Weeks, 2013, *arXiv:1303.4627*.
36 P. N. Pusey, E. Zaccarelli, C. Valeriani, E. Sanz, W. C. K. Poon, and M. E. Cates, *Philos. T. R. Soc. A*, 2009, **367**, 4993-5011.
37 G. H. Bogush, M. A. Tracy, and C. F. Zukoski, *J. Non-Cryst. Solids*, 1988, **104**, 95-106.
38 A. van Blaaderen and A. Vrij, *J. Colloid Interf. Sci.*, 1993, **156**, 1-18.
39 M. Raşa and A. P. Philipse, *Nature*, 2004, **429**, 857-860.
40 V. M. Masalov, N. S. Sukhinina, E. A. Kudrenko, and G. A. Emelchenko, *Nanotechnology*, 2011, **22**, 2757.
41 C. Song, P. Wang, and H. A. Makse, *Nature*, 2008, **453**, 629-632.
42 R. Piazza, S. Buzzaccaro, and E. Secchi, *J. Phys.: Condens. Matter*, 2012, **24**, 284109.
43 M. Raşa, B. H. Erné, B. Zoetekouw, R. van Roij, and A. P. Philipse, *J. Phys.: Condens. Matter*, 2005, **17**, 2293-2314.
44 P. J. van Zwol, G. Palasantzas, and J. Th. M. DeHosson, *Phys. Rev. E*, 2009, **79**, 041605.
45 D. Bonn, H. Tanaka, G. Wegdam, H. Kellay, and J. Meunier, *Phys. Rev. Lett*, 1998, **45**, 52-57.
46 W. C. K. Poon, E. R. Weeks, C. P. Royall, *Soft Matter*, 2012, **8**, 21-30.
47 J. Brujic, personal correspondence (2013).
48 M. C. Jenkins, M. D. Haw, G. C. Barker, W. C. K. Poon, and S. U. Egelhaaf, *Soft Matter*, 2011, **7**, 684-690.
49 K. Hitti and M. Bernacki, *Appl. Math. Model.*, 2013, **37**, 5715-5722.
50 W. M. Visscher and M. Bolsterli, *Nature*, 1972, **239**, 504-507.
51 P. C. Hiemenz and R. Rajagopalan, *Principles of Colloid and Surface Chemistry* (3rd Ed., CRC Press, 1997).
52 V. V. Yaminsky, P. M. Nanikashvili, Th. Götze, H. Sontag, and E. D. Shchukin, *Kolloidn. Zh.*, 1986, **48**, 1205.
53 M. H. Lee and E. M. Furst, *Phys. Rev. E*, 2006, **74**, 031401.
54 R. D. Kamien and A. J. Liu, *Phys. Rev. Lett.*, 2007, **99**, 155501.
55 P. N. Segré, F. Liu, P. Umbanohowar, and D. A. Weitz, *Nature*, 2001, **409**, 594-597.
56 A. R. Dexter and D. W. Tanner, *Nature-Phys. Sci.*, 1972, **238**, 31-32.
57 H. J. H. Brouwers, *Phys. Rev. E*, 2006, **74**, 031309.
58 D. M. E. Thies-Weesie and A. P. Philipse, *J. Colloid Interf. Sci.*, 1994, **162**, 470-480.
59 A. Donev, I. Cisse, D. Sachs, E. A. Variano, F. H. Stillinger, R. Connelly, S. Torquato, and P. M. Chaikin, *Science*, 2004, **303**, 990-993.

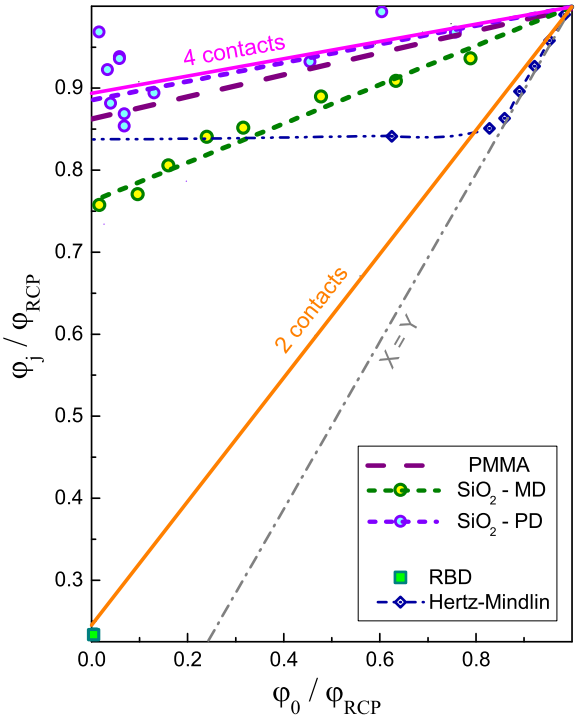

Fig. 3 Particle volume fractions in solid sediments φ_j increase for denser initial fluids, exhibiting a (roughly) linear trend for the monodisperse charge-stabilized SiO_2 colloids (green circles, marked SiO_2-MD). The slope of these data is slightly larger than for the hard frictional PMMA spheres [1] (purple dashes), indicating that sticky van der Waals contacts between SiO_2 colloids provide mechanical stabilization to structures with low connectivity. Correspondingly, $\varphi_j(0) = 0.49$ for SiO_2-MD, well below $\varphi_j(0) = \varphi_{RLP} \approx 0.55$ of PMMA. A solid of even lower density is formed by hit-and-stick random ballistic deposition (RBD) of silica particles in vacuum [2] (green rectangle at $\varphi_0 \to 0$). The intersection of each data set with $\varphi_j = \varphi_0$ (dash-dotted grey line) sets the upper limit on the corresponding sediment densities, yielding $\varphi_j \leq \varphi_{RCP} \approx 0.64$ for all experimental data in this plot. All data are normalized by $\varphi_{RCP} = 0.64$, except for the theoretical '2 contacts' and '4 contacts' lines, normalized by 0.537 and 0.505, respectively (see text). The sediment densities of polydisperse silica spheres [SiO_2 - PD, cyan circles and dashes; see $P(\sigma)$ in Fig. 6] exhibit a significantly reduced $\varphi_j(\varphi_0)$ slope. Theoretical densities of jammed athermal gravitation-less Hertz-Mindlin spheres [41], at high friction ($\mu \to \infty$), are non-linear in φ_0; yet, these data converge, within the experimental accuracy, to φ_{RLP} and φ_{RCP} of hard frictional PMMA colloids.

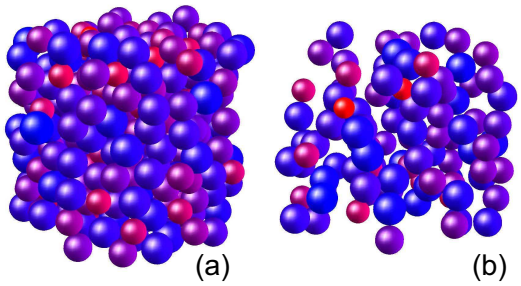

Fig. 4 Simulated structure of the sediment, based on the experimental $P(\sigma)$ of the polydisperse sample, see Fig. 6; here $\varphi_0 \to 0$. (a) Each particle is supported by no less than two other particles, so that the number of contacts is $Z \approx 4$. (b) Each particle is supported by no less than one other particle ($Z \approx 2$). Note the string-like appearance of the sediment. Sedimentation direction is downward in these plots. The structures represent cylindrical cuts from the center of the simulation cell. Importantly, the experimental differences between sediments of SiO_2 and PMMA spheres in Fig. 3 are much more subtle, corresponding to only $\sim 10\%$ change in Z. Color coding is used to emphasize the differences in diameters between the particles.

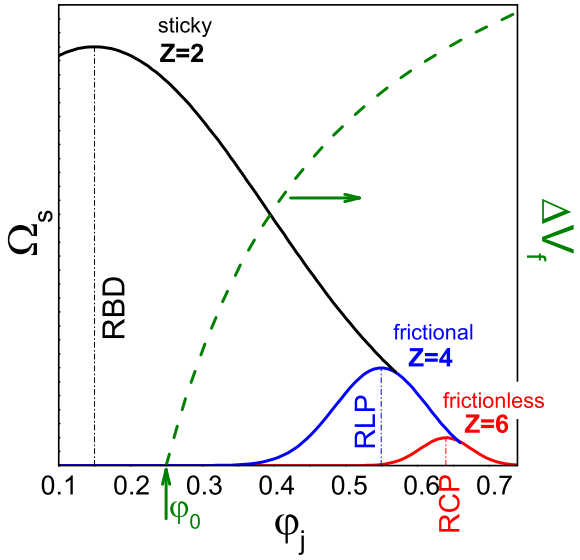

Fig. 5 Tentatitve schematic representation of the number of mechanically-stable microscopic states Ω_s (solid lines) in frictionless (red), frictional (blue), and sticky (black) particles, as a function of the packing density. The maxima correspond to the most probable average packing densities, for a macroscopic sediment formed from a fluid at $\varphi_0 = 0$, where all correlations are missing; thus, frictionless particles pack to $\varphi_j = \varphi_{RCP} \approx 0.64$, frictional ones - to $\varphi_{RLP} \approx 0.55$, and sticky ones - to $\varphi \approx 0.15$, as in random ballistic deposition (RBD) experiments[2]. Note, all stable frictionless packings are necessarily stable also in presence of friction; similarly, all frictional packings necessarily remain stable if cohesive interactions are turned on. Packings formed from a finite density $\varphi_0 > 0$ fluid are not chosen on random from the Ω_s distribution. Instead, the probability for a packing density φ_j is biased by the free volume in the fluid at φ_0, measured with respect to the jammed packing at φ_j (green dashed line, for $\varphi_0 = 0.25$); thus, loosest packings, where $\varphi_j < \varphi_0$, are completely excluded; also, there is a preference for the densest packings, so that the average φ_j increases with φ_0, as in Fig. 3.

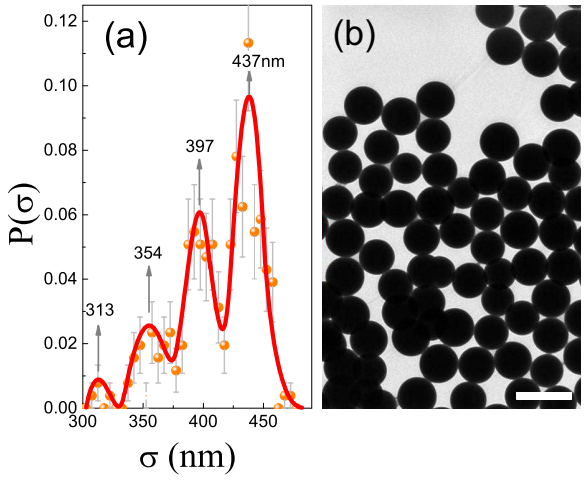

Fig. 6 (a) A very broad, skewed, four-peaked particle size distribution, is observed for our 'polydisperse' sample, the TEM image of which is shown in section (b). Sediment packing fractions of these spheres are increased dramatically, compared to the monodisperse case; moreover, they exhibit a very weak dependence on φ_0, emphasizing that a careful control of polydispersity is necessary in studies of solid non-crystalline sediments. The scale bar length is 600 nm.

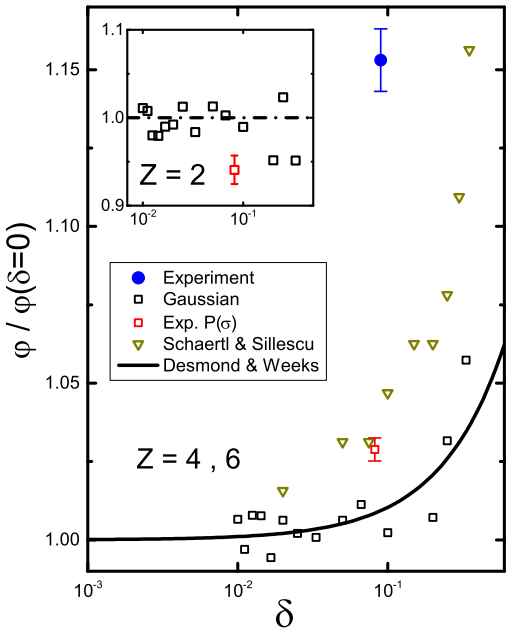

Fig. 7 The simulated density of loosely packed sediments $\varphi_j(0)$ of spheres, with their sizes following a Gaussian distribution (open squares), is plotted as a function of the polydispersity δ; the data are normalized by the density at $\delta = 0$. The resulting values significantly underestimate the experimental result (solid blue circle), obtained for the skewed $P(\sigma)$ in Fig. 6(a). Taking the exact shape of $P(\sigma)$ into account, as also accounting for particle size segregation in the centrifuge, does not significantly change the results (open red square). The same simulations are carried out for the number of contacts per particle being $Z = 4$ (main panel) and $Z = 2$ (inset); in both cases, the shift in density compared to the monodisperse case is too small, compared with the experiment. Open dark yellow triangles are computer simulated RCP densities (for $Z = 6$), obtained by Schaertl and Sillescu [34] for a Gaussian particle size distribution. RCP values predicted by simulations of Desmond and Weeks [35] are shown in a solid line, for the same skewness as in Fig. 6(a) and $Z = 6$. The experimental φ_{RCP} (Fig. 3) do not change significantly, within the experimental scatter, for the polydisperse samples, in agreement with the theory [34,35]; yet, there is a clear experiment-theory disagreement as for the value of $\varphi_j(0)$, calling for more adequate theoretical work to be carried out in future.